



Effect of individual and hybrid additions of Al₂O₃ NP and CNTs on the mechanical strengthening of aluminum-bronze alloy

E. A. Eid¹ · M. Ragab¹Received: 13 October 2019 / Accepted: 6 January 2020 / Published online: 10 January 2020
© Springer Nature Switzerland AG 2020

Abstract

Aluminum bronze metallic composite (ABMCs) alloys were fabricated via the powder metallurgy technique. The present work has been incorporated an individual as well as hybrid additions of Al₂O₃ nanoparticles and multiwall carbon nanotubes (CNTs) into ABMCs. Microstructural characteristics and mechanical properties and sliding wear behavior plus some of the physical properties such as density, electrical conductivity, and thermal conductivity of the composite alloys have been studied. Microstructure features were discovered by utilizing FE-SEM and XRD measurements. The addition of 2 wt% of CNTs was caused more uniform distributed refined grains, but the adding of 2 wt% Al₂O₃ was formed an agglomeration upon the active grain boundaries. Moreover, the yield stress and ultimate tensile strength of AB/Al₂O₃/CNTs hybrid composite alloy were improved up to ≈ 84% and ≈ 52%, respectively with respect to the plain monolithic alloy. Also, the hybrid addition enhanced both hardness and wear resistance by ≈ 12% and ≈ 189%, respectively. This enhancement may be attributed to the physical synergistic reinforcement of the hybrid addition and improvement of the internal microstructure as well as the Zener pinning effect which restricted the growth of the grains. Additionally, the addition of 2 wt% CNTs enhanced the electrical and thermal conductivity up to ≈ 5.3% and ≈ 22.8, respectively. Because the CNTs creating new conductive paths in the Aluminum bronze alloy.

Keywords Powder metallurgy · Aluminum bronze alloy · Hardness · Electrical conductivity · Wear rate

1 Introduction

Aluminum bronze (AB) alloys are deemed as essential materials for the various industrial scopes. These alloys have high mechanical strength, remarkable thermal behavior, good corrosion and wear resistance, as well as less expensive [1, 2]. Currently, AB alloys and their composites are utilized for several parts of automobile manufacturing and military instruments plus operating effectively in high power electronic circuits [3]. Indeed, AB alloys have limited ductility, as well as low reliability, which has restricted their use in the different applications of many technological fields. Moreover, they have a dangerous defect, where their grains coarsening with aging especially at elevated temperatures, so their internal microstructural

is unstable [4]. Consequently, the main challenge is how to develop aluminum bronze alloys without loss of their excellent mechanical characteristics and optimum electrical conductivity. It is worth to note that the fusion of Nano-sized particles (NP) is supporting the copper alloys features and increment their mechanical properties without a drop of the else physical properties [5]. Recently, a new approach of research emerged in the field of copper matrix composites (CMCs) after the production of the carbon nanotubes (CNTs) [6]. where the CNTs molecules possess an extraordinary chemical structure where their carbon atoms bonded together by sp² planner hybridization configuration. Obviously, these bonds have responsible to grant CNTs particles the excellent tensile strength, stellar thermal and electrical conductivity besides its special

✉ E. A. Eid, dr_eid_hti@yahoo.com | ¹Basic Science Department, Higher Technological Institute, 10th of Ramadan City 44629, Egypt.



physical properties [7, 8]. Though, many issues still remain such as the inhomogeneous distribution of CNTs during the mixing process. Also, the little wettability behavior between CNTs and CMCs has a negative effect on thermal stability and reduces their wear resistance [9]. For solving the current issues, Kwon et al. succeeded to incorporate the CNTs with the help of SiC NP which acts as a blending factor with Aluminum powder to obtain uniform distribution [10, 11]. Du et al. [12] notified that the addition of Al₂O₃ NP with MMCs/CNTs is increased the interfacial coherence force between CNTs and MMCs due to improving the adhesion force and augmented the wettability behavior. Cui et al. [13, 14] reported the merging of 2 wt% SiC and 11.7 wt% nickel-coated graphite within a bronze alloy enhanced the tribological results due to the strengthening effects of their ingredient. The new strategy has been used to build a hybrid synthesis of TiC and graphite powder to reinforce the CMCs by utilizing the high-power microwave sintering [15]. Koppad et al. announced the thermal and electrical conductivities are decreased after adding the MWCNTs into the Cu matrix [16]. Unfortunately, there are little works that discussed the influence of the individual and hybrid additions of CNTs and Al₂O₃ NP on the physical characteristics and their strengthening behavior for the aluminum bronze composites. Consequently, a methodical work has been performed to synthesizes the aluminum bronze alloy (Cu-11 wt% Al) via the powder metallurgy technique. Moreover, the aluminum bronze matrix was reinforced by incorporating an individual and hybrid additive of nano-sized Al₂O₃ particles and Multi-wall carbon nanotubes (CNTs). Additionally, the equipped specimens have been researched to reveal their internal microstructure by field emission scanning electronic microscope (FE-SEM) and X-ray diffraction patterns (XRD). Also, the different physical properties such as hardness, stress–strain behavior, wear characteristics, and electrical conductivity have been examined at room temperature.

2 Experimental work

2.1 The elementary materials

Powder of Copper (Cu) and Aluminum (Al) were employed as elementary material to fabricate the aluminum bronze matrix composites (ABMCs) alloy. In addition, the ABMCs were loaded by CNTs and Al₂O₃ nano-sized particles as reinforcement materials. The properties of the elementary materials that were employed to equip the tested alloys were listed in Table 1. Additionally, Fig. 1a shows the FE-SEM image of as-revised Al₂O₃ NP. Initially, the CNTs were refined by ultrasonic shaking them in a warm water bath containing an acidic aqueous solution of (3:1) H₂SO₄/HNO₃

Table 1 The morphological characteristic of materials is utilized to prepared the composite alloys

Materials	Shape	Size	Purity%	Source of materials
Copper	Powder	70 μm	99.80	Alpha Chemika, Co.
Aluminum	Powder	100 μm	99.80	Alpha Chemika, Co.
Al ₂ O ₃	Nano-size powder	50 nm	99.99	Sigma Aldrich, Co.
MWCNTs	Nano-size dust	D ₀ ≈ 25 L ≈ 35 μm	95.00	Nanotech Egypt Co.

at 60 °C for time of 3 h. Then the purify CNTs were washed and have filtered with distilled water until chemically neutralized (pH = 7.0) and were dried in an electric furnace at 50 °C. Moreover, Fig. 1b exhibits the FE-SEM image of carbon nanotubes (CNTs) after purification.

2.2 Powder metallurgy fabrication of monolithic and composite alloy

2.2.1 Blending, compacting and sintering processes

The metal powder of Cu (89 wt%) and Al (11 wt%) were mixed by a milling machine for 90 min at 300 rpm. The anhydrous acetone (2.0 wt%) was applied as a wrapping medium to help the mixing process. This process was done in a stainless-steel pot containing small stainless-steel balls ($\phi = 10$ mm). The blending powders were put in a dryer for 60 min at 80 °C to evaporate the acetone. The identical steps were repeated to prepare the composite powder loaded by CNTs and/or Al₂O₃ NP. The three composite alloys of individual and hybrid additions were equipped by their weight as listed in Table 2.

The powders metallurgy method was employed to acquire the desired composite alloys. It is worth to note that, many researchers have reported a mixing of Cu powder with CNTs is a great challenge since they are easily detached from each other [5, 9, 17]. Therefore, cyclohexane (C₆H₁₂) with paraffin wax was utilized as a lubricant substance to reduce the friction and create an appropriate medium to accomplish the mixing process between CNT with powders blend alloy [17]. The preparing powder of monolithic and composite alloys was placed into a steel die of a cavity cylinder ($\phi_{inner} = 8.0$ mm, $h = 50.0$ mm) one by one. The compact process was carried out at a pressure of 800 MPa for 90 min by utilizing the hydraulic uniaxial pressing machine supported with a high-power electric heater. Sintering is the last step to form the solid phase of composite alloys performed with heating and/or pressing at a temperature lower than the melting point of Cu/Al

monolithic alloy. Thereafter sintering process, the alloys gain good internal strength and have better properties, because the atoms of substances were diffused across the boundaries of the agglomeration particles and fuse the particles together plus create one solid piece. The sintering process of virgin specimens was carried out in vacuum muffle furnace at 900 °C for 1.5 h with heating rate of 10 °C/min and cooled at rate of 20 °C/min, and then the specimens have gradually cooled to ambient temperature and obtain the specimens as cylindrical rods of diameter

($\phi = 8.0$ mm). Furthermore, Fig. 2 summarized the graphical abstract for preparing steps and different processing carried out to obtain the desired composite alloys.

2.3 Microstructural characterization and measurements

To examine the microstructural characteristics, thick discs of alloys were grinded with silicon carbide of (SiC) emery paper (grades 120-3000) to obtain a flat free surface from

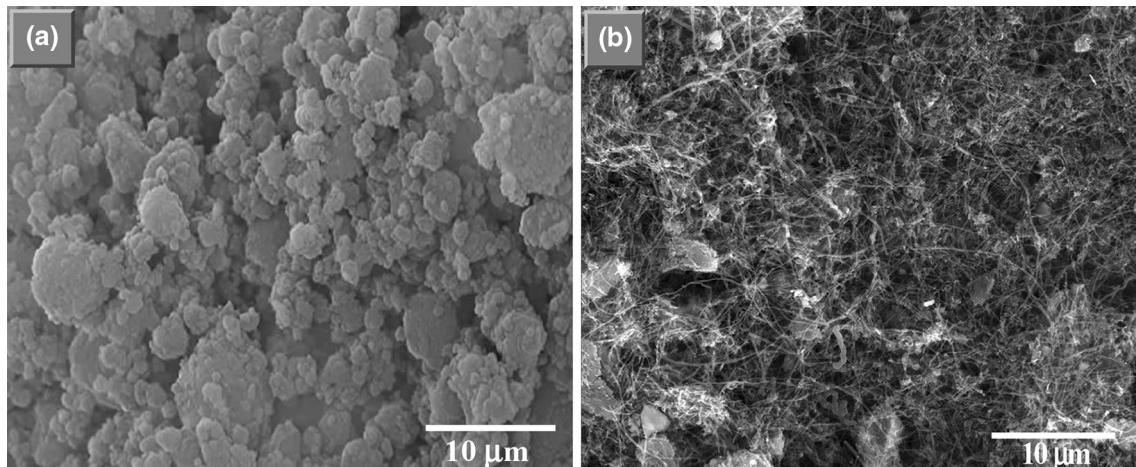
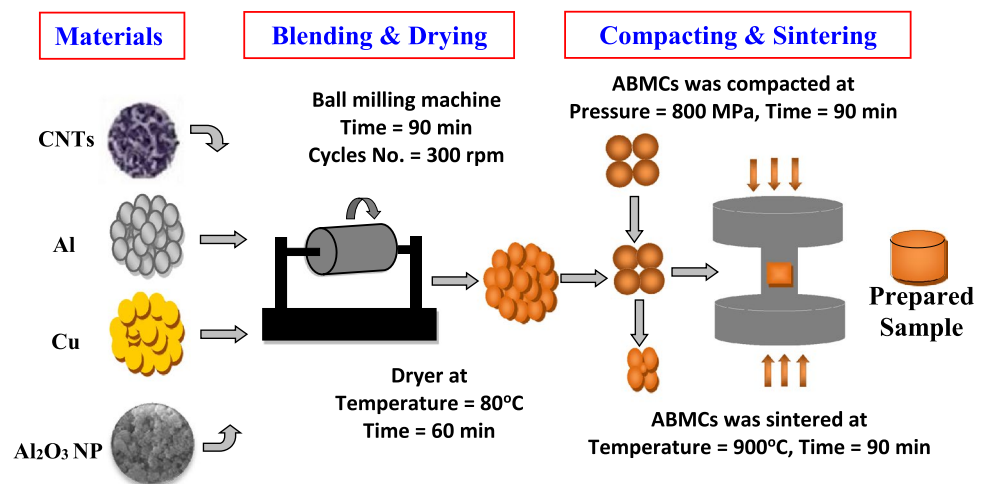


Fig. 1 **a** FE-SEM image of Al₂O₃ nano-sized particles and **b** FE-SEM image multiwall carbon nanotube (CNTs)

Table 2 Chemical composition and concentration (weight%) of studied composite alloys and their abbreviations

Alloys	Abbreviation	Cu	Al	Al ₂ O ₃	CNTs
Cu-11.0 wt% Al	AB	89.00	11.00	–	–
Cu-11.0 Al-2.0 wt% Al ₂ O ₃	AB/Al ₂ O ₃	87.00	11.00	2.00	–
Cu-11.0 Al-2.0 wt% CNTs	AB/CNTs	87.00	11.00	–	2.00
Cu-11.0 Al-1.0 Al ₂ O ₃ -1.0 wt% CNTs	AB/Al ₂ O ₃ /CNTs	87.00	11.00	1.00	1.00

Fig. 2 Graphical abstract of powder metallurgy steps for processing the investigated ABMCs



the massive scratches. Thereafter, the samples shined by using a micro-size diamond paste. Also, the samples were electro-polished at 25 V for 20 s by using electrolyte (800 ml ethanol and 200 ml perchloric acid) to remove the polluted substance. Beyond, the specimens were etched using electro-etching with oxalic acid solution with volt 6–10 V, for 30 s. The microstructure features and the distribution of the different phases were investigated utilizing the field emission scanning electron microscopy (FE-SEM; SEM-JEOL JSM5800-LV). This apparatus was equipped with a unit of an energy dispersive X-ray spectrometry (EDX) to detect the chemical configuration of the observed different phases. Furthermore, the metallographic images analysis (image J program) was applied to study the quantity and morphological features (Five digital micrographs from each sample at random locations were considered in images analysis processing). Additionally, the different metallic phases of the tested samples were determined using an X-ray diffraction instrument of monochromatic Cu-K α radiation with $\lambda = 0.154$ nm (Philips X-ray diffractometer, Model X-Pert). The scanning range was 10–90° (2 θ) with a scan step of 0.01° (2 θ)/s. The floating Archimedes principle was used to determine the real density (ρ) of the sintered samples according to the following equations [17, 18]:

$$\rho_{real} = W_a / (W_a - W_w) \quad (1)$$

where W_a and W_w are weight of the specimen in air and pure liquid of toluene, respectively, Vickers hardness measurement was carried out at a load of 1.0 kg throughout time 15 s. Lecco Vickers hardness analyzer, Model: LV 700, USA, was used to evaluate the average value of hardness of tested steel alloys. (Average of seven readings at different position was taken for each sample). Stress–strain measurements were conducted at ambient room temperature at a strain rate of $2.5 \times 10^{-3} \text{ s}^{-1}$ which equivalent to crosshead speed 5 mm/min (universal testing machine). The unidirectional of tensile tension stress was done as parallel to the cold-rolling direction of the sample. The pin-on-disk technique was utilized to measure the sliding wear behavior of tested alloys. Wire cut machine was employed to get the cylinder-shaped samples of 5 mm in diameter. Moreover, according to ASTM G99 standards for dry sliding wear tests, the sample of the flat polished contact area ($\approx 12.57 \text{ mm}^2$) was prepared. The wear tests have been performed at different nominal loads 2, 4, 6 N with sliding speed 1.5 m/s which equivalent to angular speed 250 rpm and the contact length of sliding was kept consistent at 1000 m for each composite alloy. The mass of the sample was measured before and after the test with high accuracy electronic balance (0.0001 g) to calculate the weight loss. Additionally, to get the precise result of

wear loss every individual testing was done three times and their average value was evaluated. Furthermore, the wear volume (ΔV) is calculated by Eq. (2), and the specific dry sliding wear rate (ψ) of the tested alloys is evaluated by Eq. (3) [19].

$$\Delta V = \frac{\text{Weight loss}}{\text{density}} \quad (2)$$

$$\psi = \frac{\Delta V}{P \times d} \quad (3)$$

where (P) and (d) is applied normal load (N) on the pin and the sliding distance (m), respectively. The electrical resistivity and/or electric conductivity of tested alloys was measured by Motwane Digital Micro ohm meter (LR-2045) which is capable of measuring very low resistances in micro ohm as low as 0.1 $\mu\Omega$. Then, the electric conductivity (σ) is dependent on electrical resistance (R) of the specimen was evaluated using the following formula [18, 20].

$$\sigma = \frac{L}{A \times R} \quad (4)$$

where L and A are the length between the ohmmeter terminals and area of measured sample, respectively.

3 Results and discussion

3.1 Microstructure and phases characteristics

Figure 3a–f shows the diffractograms of XRD outcomes for the initial pristine powders of Al $_2$ O $_3$ NP, CNTs, and as prepared composite alloys. Figure 3a, b exhibit the main diffraction peaks of Al $_2$ O $_3$ and CNTs, respectively. Figure 3c shows the diffraction peaks of the sintered AB monolithic alloy, it contains the fundamental peaks of α -Cu phase that observe at $2\theta = 43.8^\circ$, 50.4° , and 75.7° . Additionally, weak peaks belonging to AlCu $_3$ appeared at $2\theta = 47.2^\circ$ that can be attributed to the complex reaction during sintering. Figure 3d, e display XRD patterns of AB/Al $_2$ O $_3$ and AB/CNTs samples, respectively. Moreover, Fig. 3f reveals two small peaks of Al $_2$ O $_3$ at 34.95° 57.4° and another little peak for CNTs at 24.1° . this observation confirms the incorporation of Al $_2$ O $_3$ NP as well as CNTs within Al-bronze matrix alloy. Generally, all diffraction patterns demonstrate the formation of metallic phases of composite alloys. Additionally, Fig. 4a, b shows SEM photograph and EDX elemental analysis of different phases in sintering monolithic AB alloy, respectively. EDX analysis in Fig. 4b confirms that the Al-phase is light gray regions and the Cu-phase is dark grey zones. Also Fig. 4a reveals the finer Al grains

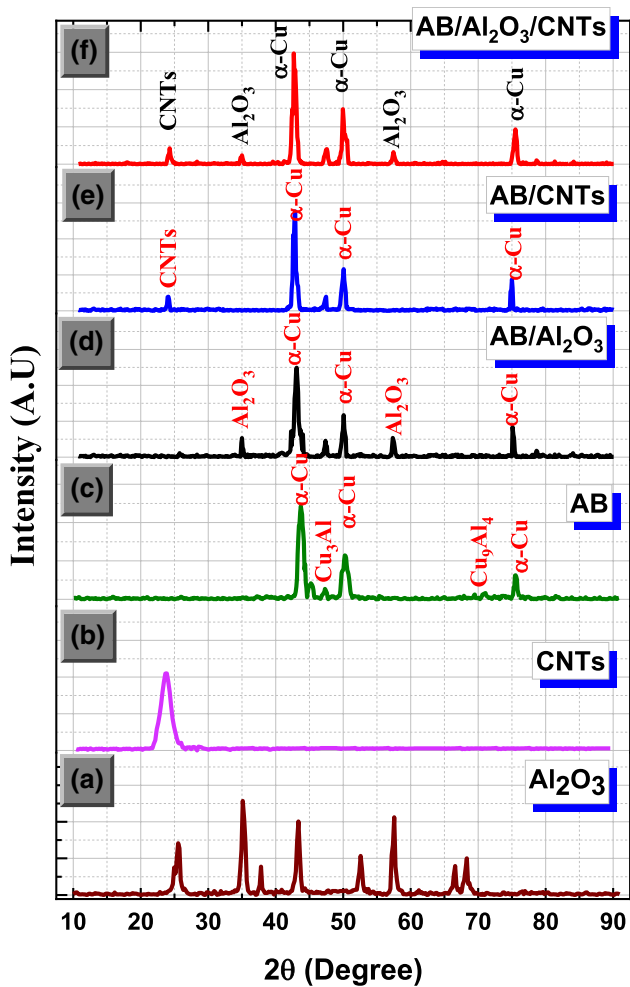


Fig. 3 X-ray diffraction patterns of pristine powders of **a** Al_2O_3 , **b** CNTs, **c** AB monolithic alloy, **d** $\text{AB}/\text{Al}_2\text{O}_3$ composite alloy, **e** AB/CNTs composite alloy, and **f** $\text{AB}/\text{Al}_2\text{O}_3/\text{CNTs}$ composite alloy

inhabiting the empty spaces between Cu grains and a little number of voids dispersed throughout AB matrix alloy due to the mutual uniform distribution of phases. It is Worthy note that, the Al-bronze alloys characterize by forming several sorts of intermetallic compounds (IMCs) due to the high affinity between Cu and Al element, especially at elevated temperatures more than 120 °C. Based on the study of the Cu-Al phase diagram, five species kinds of IMCs (CuAl_2 , CuAl , Cu_3Al , Cu_4Al_3 , Cu_3Al_2 , and Cu_9Al_4) recognized at the temperature range 350–500 °C [2]. Otherwise, microstructural examinations for all ABMCs alloys have cleared that, IMC was not formed in their matrices. On the other hand, Cu_3Al and Cu_9Al_4 IMCs were detected at 47.2° and 70.9°, respectively, in the XRD pattern of AB monolithic alloys (Fig. 3c). Figure 5a displays that the addition of 2.0 wt% Al_2O_3 has a great impact on the morphology and the distribution of the grain of $\text{AB}/\text{Al}_2\text{O}_3$ composite alloy. This figure displays finer grains and nearly homogenous texture besides little voids and agglomerated shapes accumulated along the coarse grain boundaries. The EDX elementals analysis in Fig. 5b confirms that the agglomerated white dots embedded in the AB matrix are Al_2O_3 particles. Moreover, Fig. 6a shows the effect of 2 wt% CNTs addition on monolithic alloy. It is clear that the composite matrix has more refining grains and more orderly texture. This enhancement in microstructure related to the ability of the Al phase to induce the formation of the physical bonding between CNTs and Cu phases that play a necessary factor in developing the physical and mechanical characteristics [12, 20]. Figure 6b reveals the EDX elemental analysis of a very dark black zone that appears in the SEM micrograph in Fig. 6a. The elemental analyses confirm that 23.8 at% of the carbon phase associated with 66.61 at% and 8.1 at% of copper and aluminum phase, respectively. This

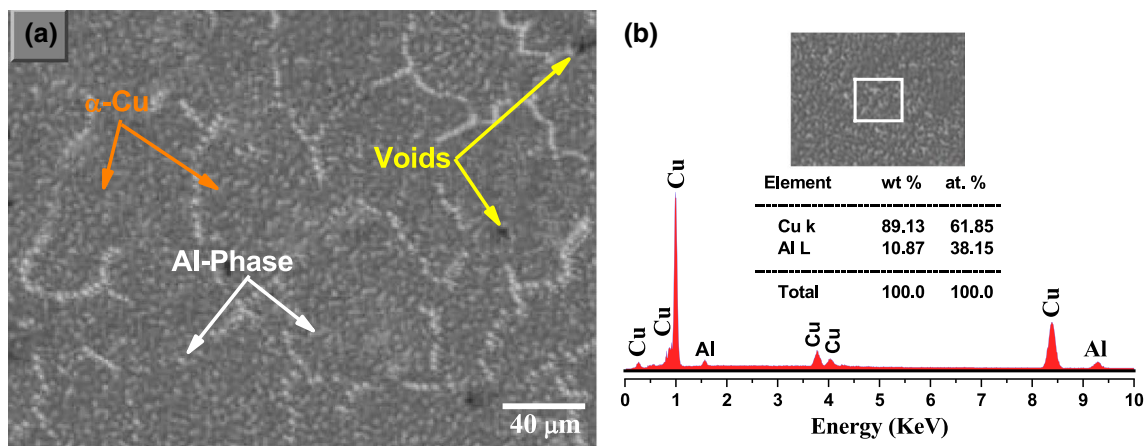


Fig. 4 **a** SEM image of AB monolithic alloy, and **b** EDX spectroscopy with elemental analysis of the white square region at the present image

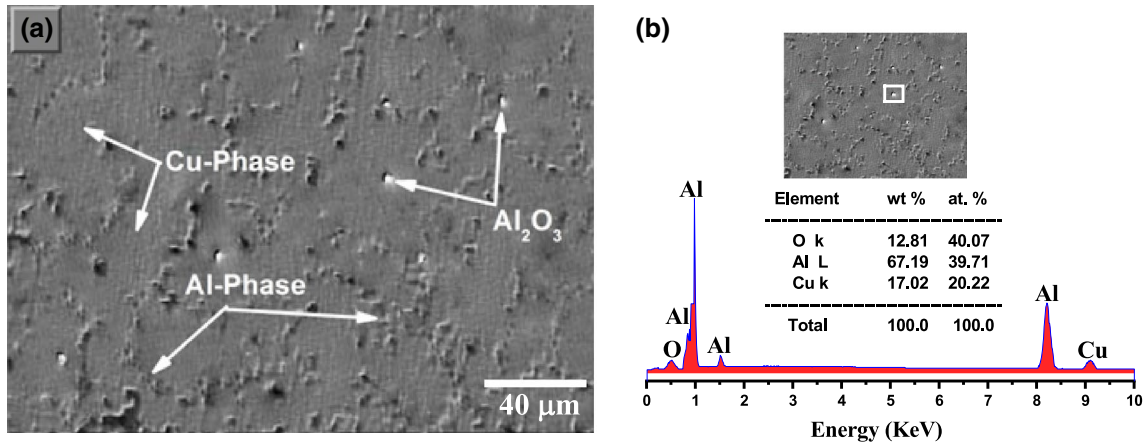


Fig. 5 a SEM image of AB/Al₂O₃ composite alloy, and b EDX spectroscopy with the elemental analysis of the white dots at the present image

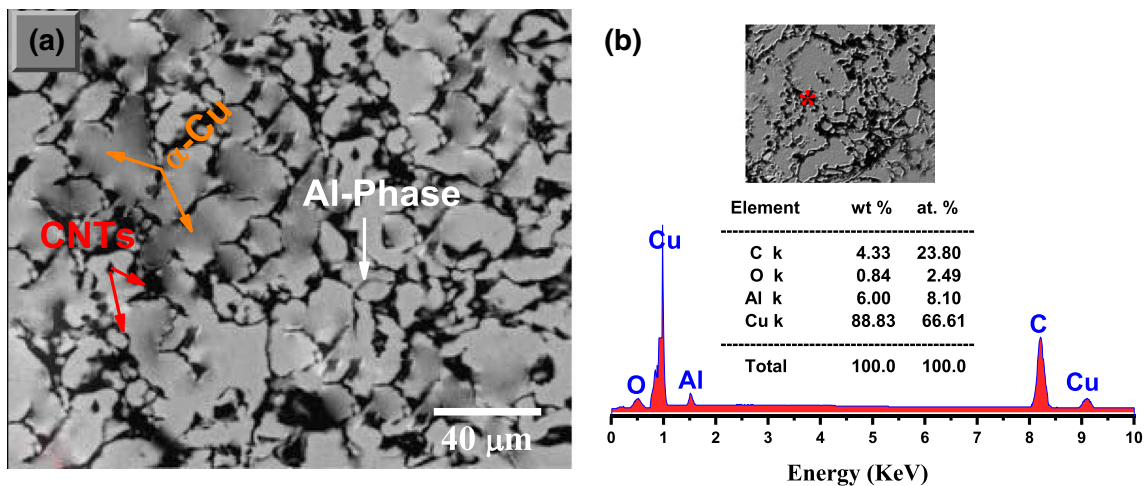


Fig. 6 a SEM image of AB/CNTs alloy, and b EDX spectroscopy with the elemental analysis of the dark motifs at the present image

outcome refers to the monolithic grains that have been covered by CNTs that led to restricted their growth. Figure 7a shows the microstructure of the AB/Al₂O₃/CNTs hybrid composite alloy. Notably, the hybrid addition has a great positive impact and gathered both benefits of their individual additions. Therefore, the AB/Al₂O₃/CNTs hybrid alloy has an excellent homogenous distribution plus soft edge grain boundary as well as their intrinsic voids nearly absent. Furthermore, some micro-sizes particles of Al₂O₃ and CNTs manifested within grains at the triple joint between grain boundaries due to the good mixing process between Cu, Al, and ingredients during the blending and sintering process. Additionally, Fig. 7b, c exhibits the EDX elemental chemical analysis of the different phases that were appeared in the SEM image of the hybrid composite alloy. These analyses have confirmed the presence of the different phases that discussed in the above section.

3.2 Mechanical characteristics

3.2.1 Hardness and density

Figure 8 displays the measured values of microhardness of the tested composite alloys at room temperature. The outcomes of the hardness referred that AB/Al₂O₃, as well as AB/CNTs alloy, has a higher hardness than AB monolithic alloy. Also, the addition of the Al₂O₃ nanoparticles has more effective hardening than the addition of CNTs. The CNTs have low bonding behavior with the AB composite alloy owing to its poor wetting with the Cu phase as well as their large surface area prohibits the motion of Cu or Al atoms during sintering process [18, 20]. Moreover, Fig. 8 shows the values of theoretical and real density (ρ_{real}) of studied composite alloys, the results have indicated that the values of calculated and real density are nearly closed to each other. Furthermore,

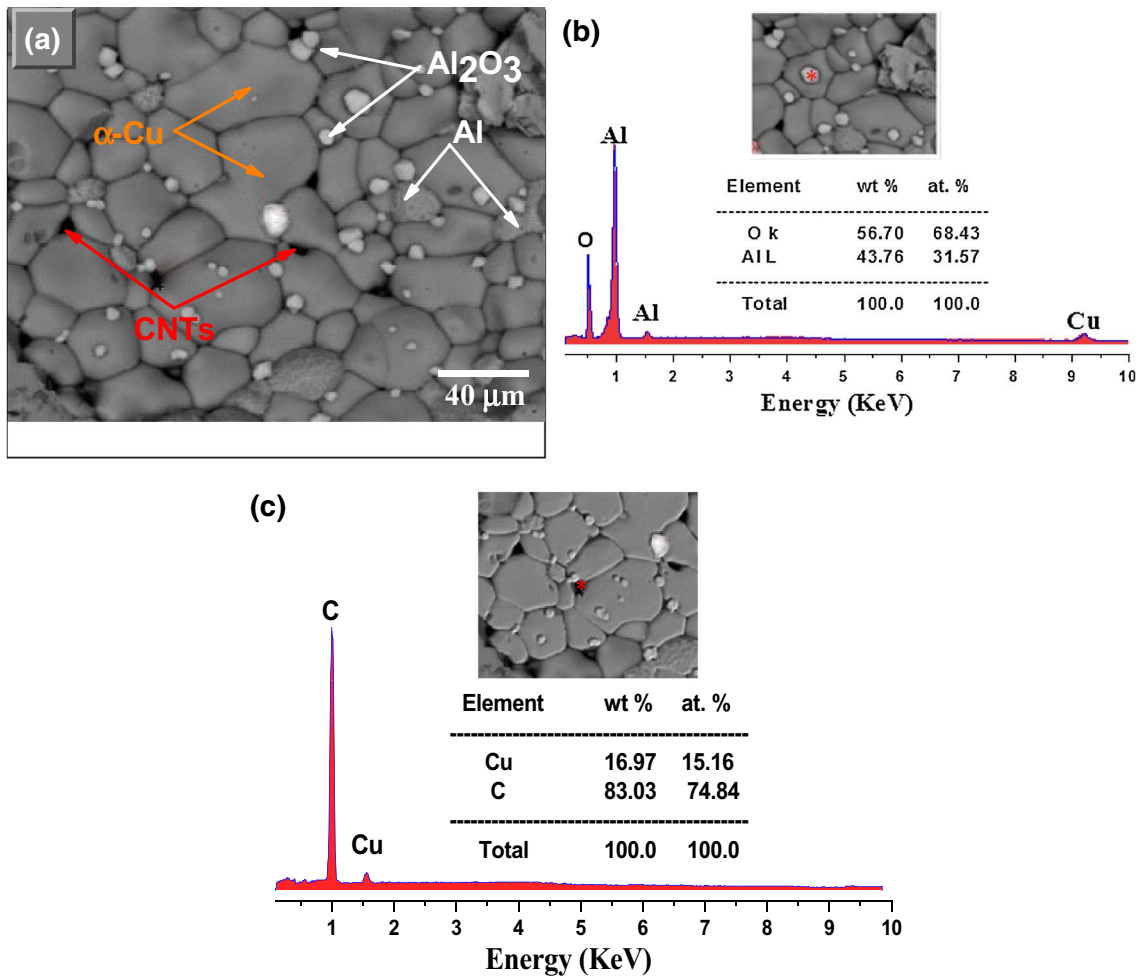
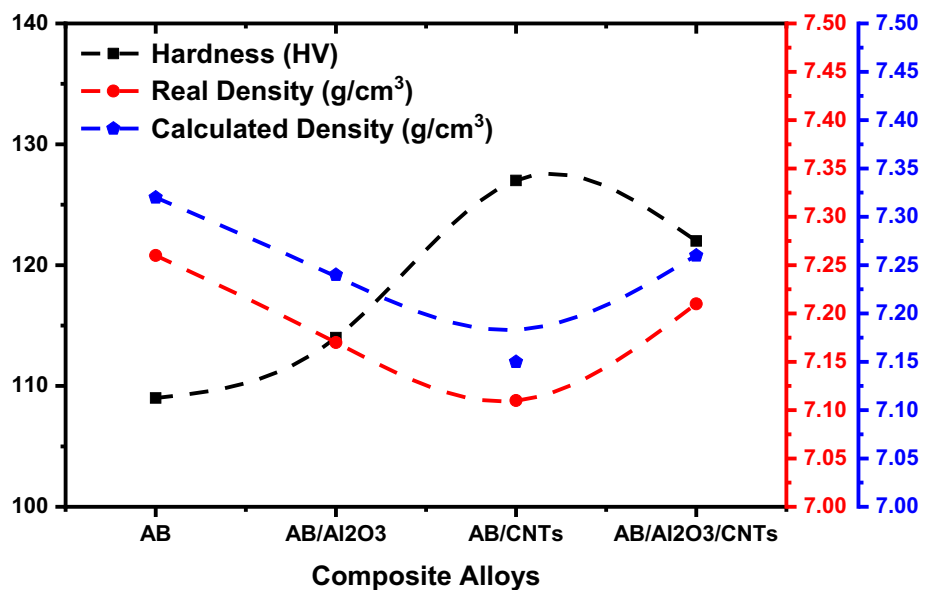


Fig. 7 a SEM image of AB/Al₂O₃/CNTs hybrid composite alloy, b EDX spectroscopy with the elemental analysis of the white gray dots at the present image, and c EDX spectroscopy with its elemental configuration of dark spot

Fig. 8 The values of hardness, real, and calculated density of the studied composite alloys



the density of AB/CNTs composite alloy slightly lowered than that of the other composite alloys. Additionally, the density of AB/Al₂O₃/CNTs hybrid composite alloy was increased than that containing an individual addition of Al₂O₃ nanoparticles or CNTs. These findings can be interpreted according to the different magnitudes of the thermal expansion coefficient (CTE) of ingredients and the AB matrix. Also, the large alteration between the density of AB Matrix (7.56 g/cm³) and their additives ($\rho_{Al_2O_3} = 3.98 \text{ g/cm}^3$ and $\rho_{CNTs} = 1.8 \text{ g/cm}^3$) lead to a decrement of the density of the composite alloys [20]. Thus, the augment in the density of AB/Al₂O₃/CNTs alloy owing to merging a minor amount of CNTs that gives a uniform dispersion plus the adding of Al₂O₃ NP leads to enhance density due to filling up the intrinsic voids of AB alloy.

3.2.2 Tensile stress–strain characteristics

Figure 9a shows the typical tensile true stress–strain curves of the studied composite alloys that strained by rate $2.5 \times 10^{-3} \text{ s}^{-1}$ at room temperature. The yield stress (YS), ultimate tensile strength (UTS) and ductility (EI%) of the tested alloys are extracted from their curves and summarized in Fig. 9b. The AB monolithic alloy exhibits the lower values of yield strength ($\sim 181.4 \text{ MPa}$) and the ultimate tensile strength of ($\sim 306 \text{ MPa}$) but has a higher value of ductility ($\sim 21.5\%$) comparing with the other composite alloys. Meanwhile, AB/Al₂O₃/CNTs hybrid composite alloy reveals a higher value of YS, UTS than the other composite alloys. Its UTS increased to approximately 52% meanwhile its ductility lowered nearly 21% than the values of the AB monolithic alloy. Generally, the augmentation of hardness, YS, and UTS after the addition of Al₂O₃ nanoparticles and/or CNTs can be attributed to the synergetic reinforced nature of nanoparticles as well as their pinning effect on the grain boundaries of the AB matrix [12]. Furthermore, the increase in hardness observed after additions of CNTs and/or Al₂O₃ can be correlated to the strengthening effect of them. Since, the mechanical properties of CMCs are dependent on several factors such as (1) physical and chemical nature of reinforcement particles, (2) dislocation density and their distribution, and (3) grain size plus their uniform distribution. Additionally, the thermal mismatch between different ingredients of CMCs leads to create strain fields that hump the mobility of dislocation and strengthens the CMCs matrix [21]. Thus, based on the rule of strengthening metallic mixtures and the higher hardness values of our additives (CNTs and Al₂O₃) we can interpret the improvement of the tensile parameters of the tested alloys.

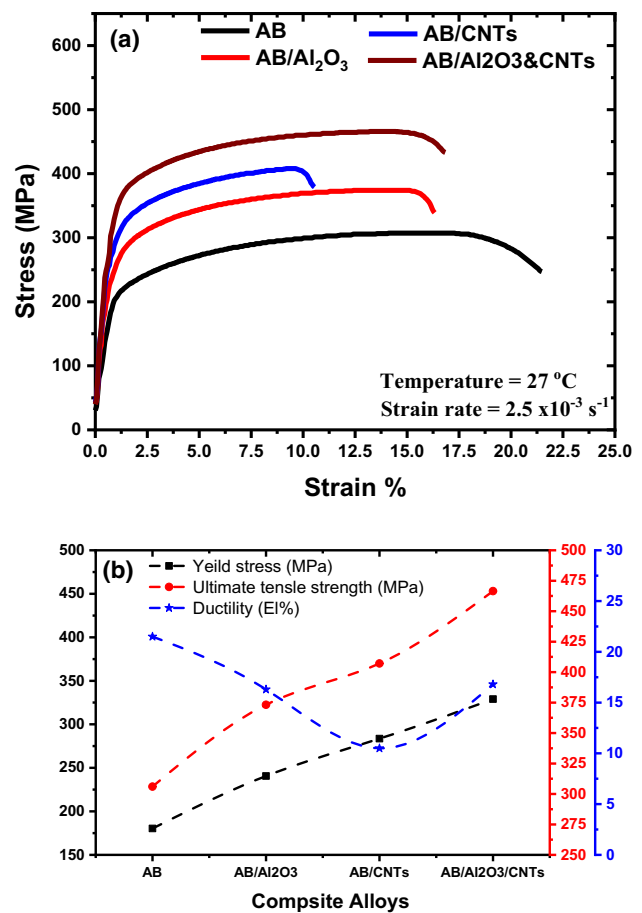
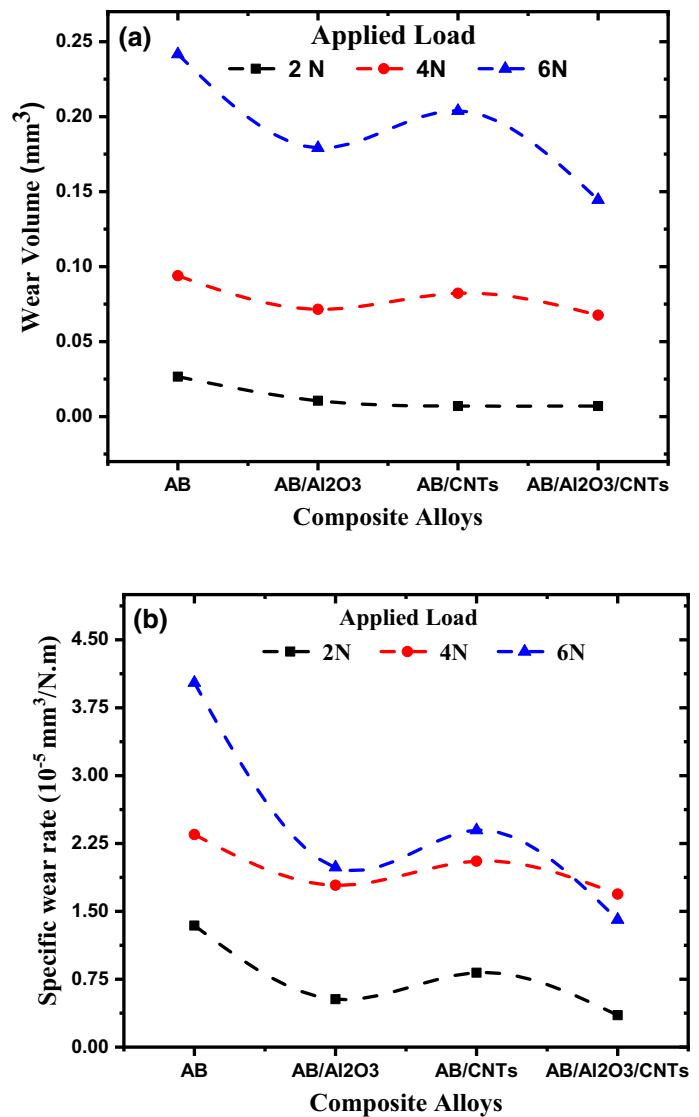


Fig. 9 **a** Stress–strain behavior of tested composite alloys strained at $2.5 \times 10^{-3} \text{ s}^{-1}$ at room temperature and **b** the yield stress, ultimate tensile strength and ductility of the tested composite alloys

3.3 The sliding wear characteristics

The wear behavior of the tested composite alloys was studied by measuring the volume loss by sliding wear and the equivalent of wear rate at different applied loads. Figure 10a displays the volume wear loss of the studied alloys by employing a dry sliding wear test. The graph reveals a slight difference in wear loss of AB monolithic alloy and the other composite alloys under the various applied loads. Obviously, the volume wear loss behavior of tested composite alloys is largely influenced by applied load and nearly nondependent on kind of the nano addition. Also, the monolithic and hybrid composite alloys show extraordinary behavior with respect to the volume wear loss values at any applied load. Figure 10b exhibits the specific wear rate of the studied composite alloys dependence on the values of applied loads. The wear rate was measured to be $4.03 \times 10^{-5} \text{ mm}^3/\text{Nm}$ for monolithic AB alloy and $1.41 \times 10^{-5} \text{ mm}^3/\text{m}$ for the hybrid composite alloy at the applied load of 6 N. Generally, an individual

Fig. 10 **a** The wear volume of composite alloys at different loads, **b** The specific wear rate of composite alloys at different loads



addition of CNTs and/or Al₂O₃ NP remarkably decreased the wear rate and leading to improve the wear resistance of the composite alloys comparing to the AB alloy. Hence, the wear loss and wear rate dramatically decrement with the hybrid addition of % Al₂O₃ NP and CNTs. This is due to the existence of CNTs aggregates as well as the Al₂O₃ NP have been smeared the interfacial surface of counterparts of pen and counterpart of hardening wear disk. Hence, these aggregates act as good solid lubricants that lowered the friction behavior [22]. On another hand, based on the atomic bond's theory, the aggregates of CNTs and Al₂O₃ nanoparticles have hexagonal structure and its atomic bonds in basal planes are a very strong covalent bond, but atomic bonds between basal planes are weak physical Van-der-Waals bond. Therefore, these weakened bonds are easily destroyed by shearing strength during dry sliding wear and leading to a decrease in the value of friction coefficient and/or wear rate [23]. Additionally, the

reduction in wear rate is related to the augmentation of hardness according to the Archard law of sliding wear that is obtained by Eq. (6) [24].

$$\Delta V = K \frac{FD}{H} \quad (5)$$

where (ΔV) is loss volume during sliding wear distance (D) under applied normal load (F), K is dimensionless wear coefficient, and (H) is the hardness of the composite alloy. Generally, the sliding wear resistance ($R_w = H/K$) of composite alloys is directly proportional to its hardness (H).

3.4 Electrical and thermal conductivity

Figure 11 depicts the values of the electrical conductivity (σ) of the studied composite alloys at room temperature ($T = 27^\circ\text{C}$). The AB/Al₂O₃ composite alloy has revealed the lowest values of electrical conductivity (σ)

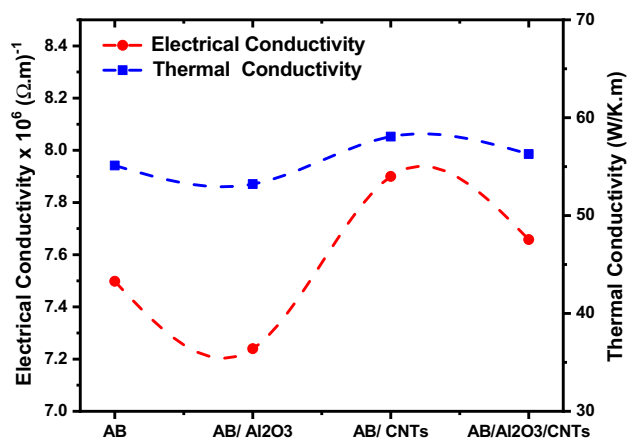


Fig. 11 The electrical and thermal conductivity of tested composite alloys at room temperature

comparing to the other alloys. This small dropping in (σ) related to the intrinsic properties of Al_2O_3 NP which has a low electrical conductivity [20]. Furthermore, AB/CNTs composite alloy has exhibited the highest electrical conductivity due to the existence of the conductive CNTs particles which create new conducting paths between Cu and Al phases. The enhancement in electrical conductivity is related to unzip the nanocarbon tubes or partial crashing which occur during the metallurgical processes of preparation. This exfoliation is resulting in the creation of nanocarbon sheets which are considered as a perfect electrical and thermal conductor [8]. Moreover, the electric conductivity of hybrid composite alloy is nearly similar to the monolithic AB alloy but slightly lower than AB/CNTs composite alloy. This decrement is due to Al_2O_3 nanoparticles is deemed as the scattering centers for the charge carriers that lead to reduce the mobility of the charge. On the other hand, Fig. 11 presents the values of thermal conductivities (κ) of the studied composite alloys. These values are calculated based on the experimental values of (σ) by utilizing the Wiedemann–Franz formula [17, 18].

$$\kappa = \alpha \sigma T \quad (6)$$

where α is Lorenz number ($2.45 \times 10^{-8} \text{ W}/\Omega \text{ K}^2$) and T is the temperature in Kelvin. Generally, the behavior of the thermal conductivity is dependent on individual and hybrid ingredient additions. Notably, the AB/ Al_2O_3 composite alloy has the lowest value of thermal conductivity comparing to the other composite alloys. The reduction in (κ) value can be correlated to the value of thermal conductivity of the Al_2O_3 NP which is considered as a thermally insulating material ($\approx 30 \text{ W}/\text{m K}$). Additionally, Cu-Al/CNTs have offered the highest value of (κ) due to the high intrinsic thermal conductivity of CNTs ($\approx 6 \times 10^3 \text{ W}/\text{m K}$) [8, 17].

4 Conclusions

Monolithic Al (11 wt%)—bronze alloy reinforced by individual and/or hybrid (2 wt%) additions of Al_2O_3 and CNTs were fabricated through the powder metallurgy technique. The main points of the research are summarized as follows:

1. The microstructure examination of composite alloys confirmed the presence of α -Cu, Al, and Cu_3Al phases were created during the sintering process. The addition of CNTs enhances the distribution and refinement of the grains, otherwise adding of Al_2O_3 NP agglomerates along the coarse grain boundaries.
2. The hybrid addition of Al_2O_3 and CNTs has a great positive effect on microstructure texture and other properties of hybrid alloy.
3. The density and hardness of AB/CNTs composite alloy has slightly decreased than monolithic AB alloy and other composite alloys due.
4. The tensile parameters (YS, and UTS) and wear rate of the hybrid composite alloy is improved due to the synergistic reinforcement of CNTs and Al_2O_3 nanoparticles.
5. The individual addition of CNTs has exhibited the highest electrical and thermal conductivity comparing to the other composite alloys.

Compliance with ethical standards

Conflict of interest The authors declare that they have no conflict of interest.

References

1. Francis R (2010) The corrosion of copper and its alloys: a practical guide for engineers. The Corrosion Society, 1440 South Creek Drive, Houston, Texas 77084. NACE International, pp 8–11. ISBN: 978-1-57590-225-8
2. Davis JR (2001) Copper and copper alloys. ASM International, Cleveland
3. Prasad NE and Wanhill RJH Aerospace materials and material technologies vol 1: aerospace materials, pp (247–251) ISSN 2509-6400, ISSN 2509-6419 (electronic) Indian Institute of Metals Series ISBN 978-981-10-2133-6 ISBN 978-981-10-2134-3 (eBook)/<https://doi.org/10.1007/978-981-10-2134-3>
4. Chu K, Jia CC, Li WS, Wang P (2013) Mechanical and electrical properties of carbon-nanotube-reinforced Cu–Ti alloy matrix composites. Phys Status Solidi 210(3):594–599. <https://doi.org/10.1002/pssa.201228549>
5. Davim JP (2014) Metal matrix composites. Walter de Gruyter GmbH, Berlin. ISBN 978-3-11-031541-7

6. Singh A, Prabhu TR, Sanjay AR, Koti V (2017) An overview of processing and properties of Cu/CNT nanocomposites. *Mater Today Proc* 4:3872–3881
7. Geim AK, Philip K (2008) Carbon wonderland. *Sci Am* 298(4):90–97
8. Popov VN (2004) Carbon nanotubes: properties and application. *Mater Sci Eng R Rep* 43(3):61–102
9. Qiao Y, Cai X, Zhou L, Pan W, Yang C, Hu C, Zhang X, Wang Z, Wu C, Zhang S (2018) Microstructure and mechanical properties of copper matrix composites synergistically reinforced by Al_2O_3 and CNTs. *Integr Ferroelectr* 191:133–144. <https://doi.org/10.1080/10584587.2018.1457383>
10. Kwon H, Saarna M, Yoon S, Weidenkaff A, Leparoux M (2014) Effect of milling time on dual-nanoparticulate-reinforced aluminum alloy matrix composite materials. *Mater Sci Eng, A* 590:338–345
11. Kwon H, Cho S, Leparoux M, Kawasaki A (2012) Dual-nanoparticulate-reinforced aluminum matrix composite materials. *Nanotechnology* 23:1–9
12. Du ZL, Tan MJ, Guo JF, Bi GJ, Wei J (2016) Fabrication of a new Al_2O_3 -CNTs composite using friction stir processing (FSP). *Mater Sci Eng, A* 667:125–131
13. Cui G, Bi Q, Niu M, Yang J, Liu W (2013) The tribological properties of bronze–SiC–graphite composites under seawater condition. *Tribol Int* 60:25–35. <https://doi.org/10.1016/j.triboint.2012.11.005>
14. Cui G, Bi Q, Yang J, Liu W (2013) Fabrication and study on tribological characteristics of bronze–alumina–silver composite under seawater condition. *Mater Des* 46:473–484. <https://doi.org/10.1016/j.matdes.2012.10.053>
15. Chandrakanth GR, Rajkumar K, Aravindan S (2010) Fabrication of copper TiC–graphite hybrid metal matrix composites through microwave processing. *Int J Adv Manuf Technol* 48:645–653. <https://doi.org/10.1007/s00170-009-2474-0>
16. Koppad PG, Rama HRA, Ramesh CS, Kashya KT, Koppad RG (2013) On thermal and electrical properties of multiwalled carbon nanotubes/copper matrix nanocomposites". *J Alloys Compd* 580:527–532. <https://doi.org/10.1016/j.jallcom.2013.06.123>
17. El-Khatib S, Shash AY, Elsayed AH, El-Habak A (2017) Effect of carbon nanotubes and nanodispersion of SiC and Al_2O_3 on mechanical and physical properties of pure copper. *Rev Adv Mater Sci* 52:126–133
18. El-Khatib S, Shash AY, Elsayed AH, El-Habak A (2018) Effect of carbon nano-tubes and dispersions of SiC and Al_2O_3 on the mechanical and physical properties of copper-nickel alloy. *Heliyon* 4:e00876. <https://doi.org/10.1016/j.heliyon.2018>
19. Sharma VK, Singh RC, Chaudhary R (2018) Experimental study of tribological behavior of casted aluminum bronze. *Mater Today Proc* 5:28008–28017
20. Pan Y, Xiao S, Lu X, Zhou C, Li Y, Liu Z, Liu B, Xu W, Jia C, Qu X (2019) Fabrication, mechanical properties and electrical conductivity of Al_2O_3 reinforced Cu/CNTs composites. *J Alloys Compd* 782:1015–1023. <https://doi.org/10.1016/j.jallcom.2018.12.222>
21. Mokdad F, Chen DL, Liu ZY, Xiao BL, Ni DR, Ma ZY (2016) Deformation, and strengthening mechanisms of a carbon nanotube reinforced aluminum composite. *Carbon* 104:64–77. <https://doi.org/10.1016/j.carbon.2016.03.038>
22. Akbarpour MR, Alipour S, Safarzadeh A, Kim HS (2019) Wear and friction behavior of self-lubricating hybrid Cu-(SiC + x CNT) composites. *Compos Part B* 158:92–101. <https://doi.org/10.1016/j.compositesb.2018.09.039>
23. Sarmadi H, Kokabi AH, Seyed Reihani SM (2013) Friction and wear performance of copper graphite surface composites fabricated by friction stir processing (FSP). *Wear* 304:1–12. <https://doi.org/10.1016/j.wear.2013.04.023>
24. Archard JF (1953) Contact and rubbing of flat surfaces. *J Appl Phys* 24:981. <https://doi.org/10.1063/1.1721448>

Publisher's Note Springer Nature remains neutral with regard to jurisdictional claims in published maps and institutional affiliations.